Magnetoelectric Coupling in Metglas/BaTiO₃/Metglas Lead-Free Magnetoelectric Composites

S. D. Patil[1], K. Y. Rajpure[1], A. M. Shaikh[2]

[1]Shivaji University, Kolhapur, India
[2]New College, Kolhapur, India
 Email: rajpure@yahoo.com, amshaikh7@gmail.com

Abstract

We report the magnetoelectric (ME) coupling in ME composites composed of $NiFe_2O_4$ (NFO) or metglas as magnetostrictive phases and $BaTiO_3$ (BTO) as piezoelectric phase, targeting lead free magetnic field sensors. NFO and BTO phases were synthesized by solid state sintering method and further characterized by using XRD and FESEM techniques. The P-E hysteresis curve shows good ferroelectric behavior with saturation polarization of P_s = 15.87 C/cm² and coercive electric field of 130 kV/cm. The ME response was characterized as a function of dc magnetic field at a fixed frequency. The transverse ME voltage coefficient, α_{ME31} shows 2 times larger magnitude than that of longitudinal ME voltage coefficient, α_{ME31}. The maximum α_{ME31} of 37 mV/cm·Oe (@H_{dc} = 250 Oe) is observed for NFO/BTO/NFO ME composites with thickness ratio of t_m/t_p = 1.0. The ME coupling is further enhanced by replacing NFO layers by highly magnetostrictive metglas layers. Metglas/BTO/metglas laminates show large α_{ME31} value of 81 mV/cm·Oe at relatively lower H_{dc} of 145 Oe. The present laminates can offer promising opportunities of engineering environmental friendly ME laminate for applications in ME devices such as energy harvester and magnetic field sensors.

Keywords

1. Introduction

Magnetoelectric (ME) laminates, the composites composed of magnetostrictive and piezoelectric layers show giant ME effects over that of natural multiferroics and particulate composites by up to several orders of magnitude [1]-[3]. The ME effect in laminate composites is realized by a stress mediated mechanical coupling be-

tween the magnetostrictive and piezoelectric layers which is often referred as a "product property" [4]. The ME effect in these laminates has drawn significant interest during the recent few years due to their extensive potential applications. To date, different laminate composites with various material compositions of piezoelectric lead zirconate titanate (PZT) or lead magnesium niobate-lead titanate (PMN-PT) and magnetostrictive Terfenol-D or metglas were reported [1]-[3] [5]. Among these laminates, PZT based ME laminates show giant magnetoelectric voltage coefficients in the order of several V/cm·Oe [1]-[3]. However, these laminates with PZT or other lead-based materials are indeed susceptible to pollution and toxicity because of Pb [6]. Hence, from the environmental point of perspective, it is highly demanding to explore the lead-free laminates and devises to replace the commonly used lead based laminates. The most commonly adopted lead free piezoelectric phase in the composites is $BaTiO_3$ due to its superior piezoelectric properties. $BaTiO_3$ has been widely used in the ME composites in the form of particulate composites or sintered ME laminates however, these composites show comparatively smaller values than the present lead free composites having 2-2 connectivity [6]-[9]. On the other hand towards the device miniaturization, there are several reports available on nanostructure composites in the shape of wires, pillars, and films [10]-[15]. However, the ME coupling of these nanostructures is much smaller to be used for device applications. It is well known that 2-2 type sandwiched ME laminates show very large ME coupling than the particulate or sintered ME composites. In recent years, metglas is widely used as a magnetostrictive material due to its very large piezomagnetic coefficient, q_{11} compared to that of other magnetostrictive materials [16]. Moreover, there is very less study on ME laminates composed of BTO and metglas as constituent phases. One can expect very large ME coupling if these two constituent phases can be combined. In this respect, herein we report symmetric ME composites made up of $BaTiO_3$ (BTO) as a piezoelectric phase and $NiFe_2O_4$ (NFO) and metglas as magnetostrictive phases.

2. Experimental

$BaTiO_3$ and $NiFe_2O_4$ phases were prepared by conventional solid state sintering process. The phase formation of $BaTiO_3$ and $NiFe_2O_4$ phases was investigated via powder X-ray diffraction (XRD) technique using (XRD-D8, Advance, Bruker-AXS). The morphological features of composites were investigated by field emission scanning electron microscopy (FESEM; Hitachi, S-4800 II, Japan). For further study, the samples in the pellet form were cut into square shape having dimensions of 5 (length) $\times$ 5 (width) $\times$ 0.3 (thickness) mm^3. The ME laminates were prepared by sandwiching $BaTiO_3$ layer between $NiFe_2O_4$ layers with thickness of 0.125 mm on the top and bottom surfaces using a silver epoxy. NFO/BTO/NFO ME laminates were prepared with different thickness ratios of $t_m/t_p = 0.8$, 1.0, and 1.2, where, t_m is the thickness of the NFO, and t_p is the thickness of the BTO, by keeping the same thickness ($t_p = 0.3$ mm) of BTO layer. Similarlly, the metglas/BTO/metglas laminates were prepared by stacking metglas layers (2605SA1, Metglas Inc., USA) with thickness of 0.025 mm on the top and bottom surfaces of the $BaTiO_3$ using a silver epoxy between magnetic and piezoelectric layers. A ME voltage across the sample, in response to a driven ac field $H_{ac} = 4$ Oe at a frequency of 1 kHz, was measured by a lock-in amplifier as a function of dc magnetic field, H_{dc}. The output voltage measurements along the out-of-plane direction (3-axis) were performed for both in-plane (1-axis) and out-of-plane (3-axis) H_{dc} (H_{ac}) orientations to estimate the transverse (α_{ME31}) and longitudinal (α_{ME33}) ME voltage coefficients, respectively. Magnetostriction, λ_{ij} was measured by a strain gauge method. Here λ_{ij} is the magnetostriction in i-axis for H along j-axis. 2.2. Maintaining the Integrity of the Specifications.

3. Results and Discussion

3.1. Structural Characterization

The XRD patterns of $BaTiO_3$ and $NiFe_2O_4$ are shown in **Figure 1**. The XRD patterns show well defined peaks with no any identified peak. The peaks in the XRD patterns were identified to be characteristics peaks of both $BaTiO_3$ and $NiFe_2O_4$ phases and indexed to be tetragonal pervoskite structure (JCPDS card No. 31-0174) and cubic spinel structure (JCPDS no. 44-1485), respectively. The lattice parameters for both the phases have been calculated. The lattice parameters for $BaTiO_3$ and $NiFe_2O_4$ were found to be $a = 3.97$ Å and $c = 4.03$ Å ($c/a = 1.01$) and $a = 8.35$ Å, respectively. The morphology and microstructure of the sintered samples were revealed by scanning electron microscopy. **Figure 2** shows the SEM images of $BaTiO_3$ and $NiFe_2O_4$ samples. **Figure 2(a)** and **Figure 2(b)** show typical SEM images of the sintered $BaTiO_3$ sample. A uniform densly packed grain size distribution ranging from 0.3 to 3 microns was observed, with well-defined crystal grain boundaries. The SEM
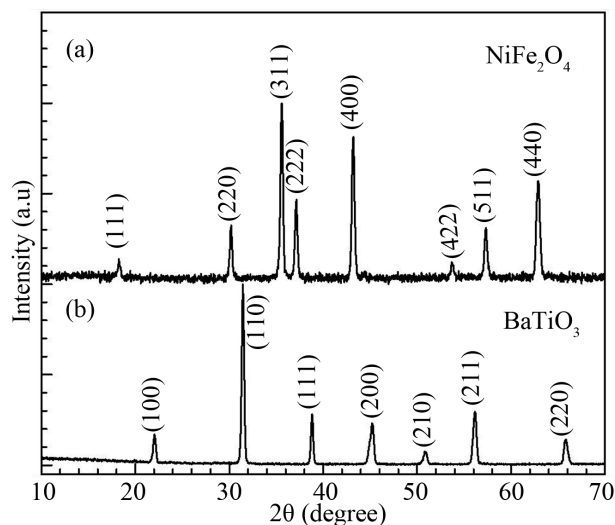
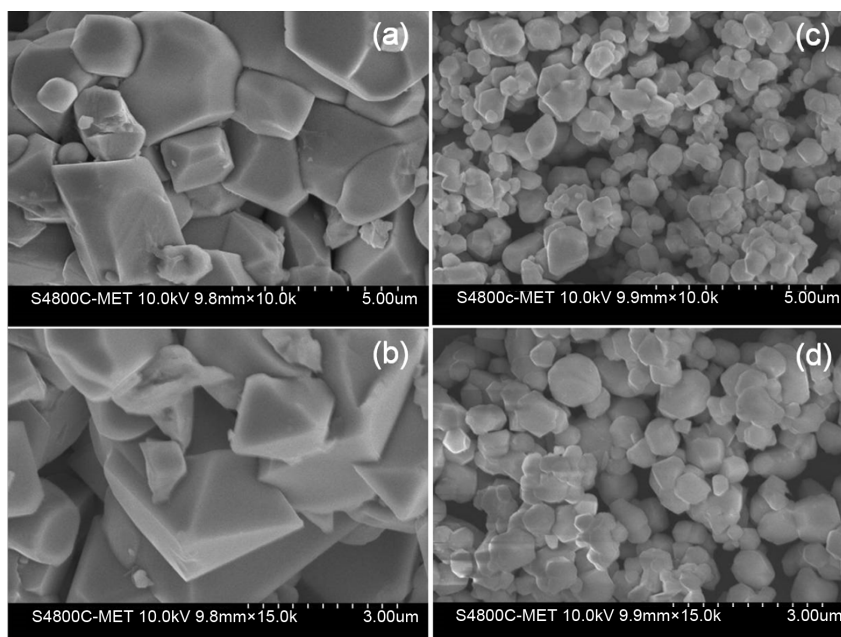**Figure 1.** XRD patterns of (a) NiFe$_2$O$_4$ and (b) BaTiO$_3$.

Figure 2. FESEM micrographs of BaTiO$_3$ (a) (b) and NiFe$_2$O$_4$ (c) (d) samples.

images of NiFe$_2$O$_4$ indicate (**Figure 2(c)** and **Figure 2(d)**) that the sample consists of uniform, spherical grains. The corresponding high-magnified SEM image shows that the spherical grains are well separated, and their sizes are less than 500 nm.

3.2. Ferroelectric Properties

In order to examine the ferroelectric nature of the BaTiO$_3$ (BTO) ceramic layer, ferroelectric P-E hysteresis behavior was measured at room temperature and shown in **Figure 3**. BTO shows the ferroelectric hysteresis behavior at room temperature. The polarization was not fully saturated possibility due to the occurrence of the electric breakdown at high electric fields. A well defined ferroelectric hysteresis loop was observed with a saturation polarization of $Ps = 15.87$ µC/cm^2 and coercive electric field and very large remanent polarization of about 130 kV/cm and 12 µC/cm^2, respectively. The observed values are consistent with that of previously reported values for BaTiO$_3$ and BaTiO$_3$ based ceramics [17] [18].

3.3. Magnetoelectric (ME) Measurement

Figure 4 shows the variation of α_{ME31} and α_{ME33} as a function of dc magnetic field, H_{dc} in response to an ac magnetic field of $H_{ac} = 4$ Oe for NFO/BTO/NFO laminates having thickness ratio of $t_m/t_p = 0.8$. As shown in figure, α_{ME} shows typical H_{dc} dependent, initially increases with increasing H_{dc}, attends a maximum, and subsequently decreases as H_{dc} increases further. Moreover, α_{ME31} and α_{ME33} show different maximum magnitudes of 27.4 and 14.73 mV/cm·Oe at different peak fields of 0.24 k·Oe and 1.5 k·Oe, respectively. The maximum value of α_{ME31} is about 2 times larger than that of α_{ME33}. The most significant observation, however, is the remarkable remnant α_{ME31} of 10 mV/cm·Oe at zero bias field ($H_{dc} = 0$ Oe). This can be attributed to the remnant magneto-striction of NFO layers at zero field [19] [20]. As α_{ME31} shows maximum value than α_{ME33}, we herein only consider α_{ME31} for further study.

Next, we focused on enhancing the α_{ME31} of the laminates by optimizing the layer thickness ratio between the NFO and BTO layers. **Figure 5** presents α_{ME31} curves of the NFO/BTO/NFO laminates with different thickness ratios, $t_m/t_p = 0.8$, 1.0 and 1.2. With increasing thickness ratio, the peak value of α_{ME31} first increases and reaches the maximum for $t_m/t_p = 1.0$ and further decreases for higher t_m/t_p. Moreover, the optimum peak field is found to be increased with increasing thickness ratio, this is because to produce the same amount of magnetostriction, the required static magnetic field has to increase as the thickness ratio increases [21]. The maximum value of $\alpha_{ME31} = 37$ mV/cm·Oe is observed for $t_m/t_p = 1.0$, which indicates that the interface coupling between the two phases is optimal when their thickness (volume) ratios are same.

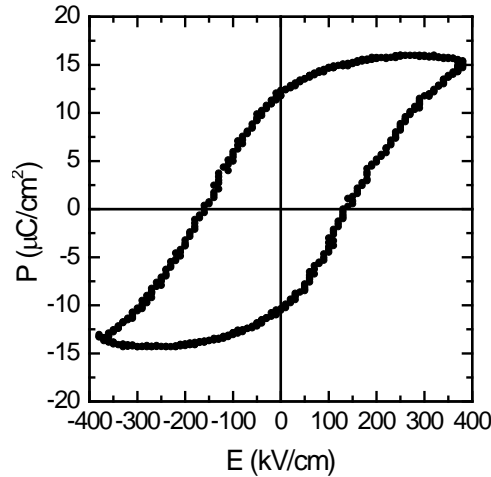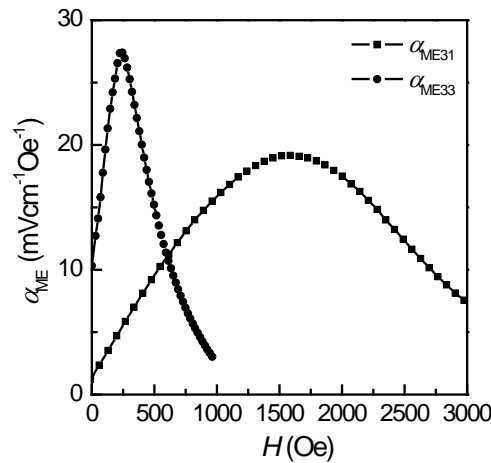**Figure 3.** Ferroelectric (P vs E hysteresis loop) properties of BaTiO$_3$ ceramic.

Figure 4. H_{dc} dependence of transverse (α_{ME31}) and longitudinal (α_{ME33}) ME voltage coefficients at a frequency $f = 1$ kHz for NFO/BTO/NFO ME laminates.

Although, we achieved large magnetoelectric coupling in the NFO/BTO/NFO laminates with $t_m/t_p = 1.0$, the values obtained for α_{ME} are still much smaller than that reported for other lead free laminates [7]. In order to further enhance the α_{ME}, we replaced NFO magnetostrictive layers by highly magnetostricitve metglas foils. Next we prepared metlgas/BTO/metglas laminates having different thickness ratio between metglas and BaTiO$_3$ layers. We indeed found that the thickness ratio of $t_m/t_p = 1.0$ shows larger value than other thickness ratios consistent with that of NFO/BTO/NFO ME laminates. Therefore in the present study we have only shown the ME data of metglas/BTO/metglas laminates with $t_m/t_p = 1.0$ and compared with that of NFO/BTO/NFO. The metglas/BTO/metglas laminates with $t_m/t_p = 1.0$ were prepared by stacking six metglas layers (2605SA1, Metglas Inc., USA) with thickness of 0.025 mm on the top and bottom surfaces of the BaTiO$_3$ using a silver epoxy. **Figure 6** shows the comparative study of H_{dc} dependence of α_{ME31} for NFO/BTO/NFO and metglas/BTO/metglas laminates. The α_{ME31} (H) for metglas/BTO/metglas also shows a qualitatively similar behaviour to that of α_{ME31} for NFO/BTO/NFO. However, the peak field for metglas/BTO/metglas is only 0.145 k·Oe, which is lower than that of NFO/BTO/NFO. Moreover, the peak value of α_{ME31} is 81 mV/cm·Oe, about 2.3 times higher in magnitude, which can be attributed to the large piezomagnetic coefficient, q_{11} of metglas than that of NFO. One can expect even much higher values of α_{ME31} for metglas based laminates as q_{11} of metglas is much larger than that of NFO. However, it is important to note that to achieve the optimized volume fraction, six metglas layers were stacked on the top and bottom surfaces of the BTO layer using a silver epoxy between each metglas layer. Therefore, under the applied magnetic field magnetostriction of the metglas is constrained by the epoxy layers in between them and as a result, q_{11} decreases and the peak field increases, which in turn reduce the overall α_{ME31}
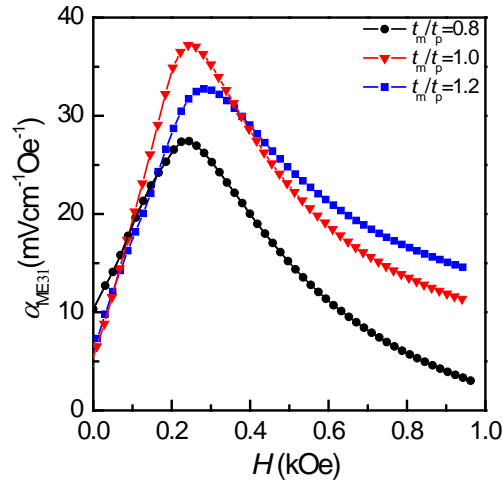

Figure 5. H_{dc} dependence of α_{ME31} for NFO/BTO/NFO ME laminates with different thickness ratios of $t_m/t_p = 0.8$, 1.0 and 1.2.
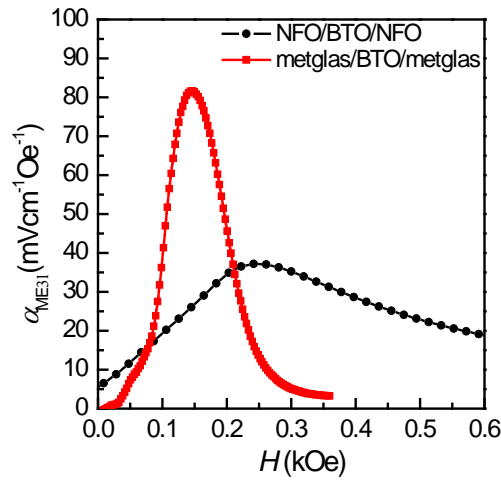

Figure 6. H_{dc} dependence of α_{ME31} for NFO/BTO/NFO and metglas/BTO/metglas ME laminates.
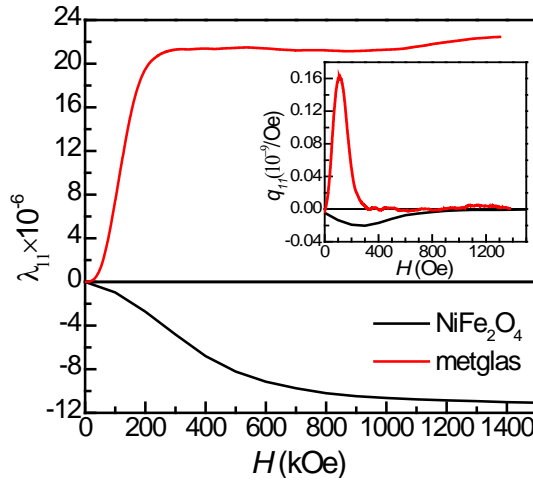
Figure 7. H_{dc} dependence of longitudinal magnetostriction (α_{ME31}) for NFO and metglas layers. Inset shows the H_{dc} dependence of piezomagnetic coefficients, q_{11} for NFO and metglas.

[21]. The H_{dc} dependence of α_{ME} can be easily understood from the magnetic-field dependent piezomagnetic coefficient, q_{ij}, *i.e.*, $d\lambda_{ij}/dH_j$, where λ_{ij} is the magnetostriction in i-axis for H along j-axis. To confirm this, we measured the H-dependent magnetostriction λ_{ij} of metglas and $NiFe_2O4$ (**Figure 7**) and calculated corresponding $q_{ij} = d\lambda_{ij}/dH_j$ (Inset of **Figure 7**). We indeed find that α_{ME31} (H) shows a qualitatively similar behavior with that of $q(H)$, having similar curvature and same peak fields. The α_{ME31} observed for metglas/BTO/metglas laminate is indeed comparable to other reported lead free laminates [7]. One can further enhance the α_{ME31} by optimizing the dimensions and/or total thickness of the laminates.

4. Conclusion

In conclusion, we have successfully synthesized and measured the ME properties of the Pb-free ME laminates. α_{ME31} is found to be larger than α_{ME33}. The α_{ME} is found to be thickness fraction dependent showing maximum for optimized thickness ration of $t_m/t_p = 1.0$ for NFO/BTO/NFO laminates. The α_{ME31} is further enhanced by replacing NFO layers by metglas. The maximum value of 81 mV/cm·Oe is observed for metglas/BTO/metglas laminates at lower H_{dc}. The present laminates offer promising opportunities of engineering environmental friendly ME laminate for applications in ME devices such as energy harvesters and magnetic field sensors.

References

[1] Fiebig, M. (2005) Revival of the Magnetoelectric Effect. *Journal of Physics D*: *Applied Physics*, **38**, R123-R152. http://dx.doi.org/10.1002/chin.200533283

[2] Nan, C.W., Bichurin, M.I., Dong, S.X., Viehland, D. and Srinivasan, G. (2008) Mulriferroic Magnetoelectric Composites: Historical Perspective, Status and Future Directions. *Journal of Applied Physics*, **103**, 031101-35. http://dx.doi.org/10.1063/1.2836410

[3] Ma, J., Hu, J., Li, Z. and Nan, C.W. (2011) Recent Progress in Multiferroic Magnetoelectric Composites: From Bulk to Thin Films. *Advanced Materials*, **23**, 1062-1087. http://dx.doi.org/10.1002/adma.201003636

[4] Suchtelen, J.V. (1972) Product Properties: A New Application of Composite Materials. *Philips Research Reports*, **27**, 28-37.

[5] Ryu, J., Carazo, A.V., Uchino, K. and Kim, H.E. (2001) Magnetoelectric Properties Inpiezoelectric and Magnetostrictive Laminate Composites. *Japanese Journal of Applied Physics*, **40**, 4948-4951. http://dx.doi.org/10.1143/JJAP.40.4948

[6] Priya, S., Islam, R., Dong, S. and Viehland, D. (2007) Recent Advancement in Magnetoelectric Particulate and Laminate Composites. *Journal of Electroceramics*, **19**, 147-164. http://dx.doi.org/10.1007/s10832-007-9042-5

[7] Bichurin, M., Petrov, V., Zakharov, A., Kovalenko, D., Yang, S.C., Maurya, D., Bedekar, V. and Priya, S. (2011) Magnetoelectric Interactions in Lead-Based and Lead-Freecomposites. *Materials*, **4**, 651-702. http://dx.doi.org/10.3390/ma4040651

[8] Patil, D.R., Sheikh, A.D., Watve, C.A. and Chougule, B.K. (2008) Magnetoelectric Properties of ME Particulate

Composites. *Journal of Materials Science*, **43**, 2708-2712. http://dx.doi.org/10.1007/s10853-008-2456-x

[9] Patil, D.R. and Chougule, B.K. (2008) Structural, Electrical and Magnetic Properties of xNiFe$_2$O$_4$+(1−x)Ba$_{0.8}$Sr$_{0.2}$TiO$_3$ ME Composites. *Journal of Alloys and Compounds*, **458**, 335-339. http://dx.doi.org/10.1016/j.jallcom.2007.03.088

[10] Srinivasan, G. (2010) Magnetoelectric Composites. *Annual Review of Materials Research*, **40**, 153-178. http://dx.doi.org/10.1146/annurev-matsci-070909-104459

[11] Oh, Y.S., Crane, S., Zheng, H., Chu, Y.H., Ramesh, R. and Kim, K.H. (2010) Quantitative Determination of Anisotropic Magnetoelectric Coupling in BiFeO$_3$-CoFe$_2$O$_4$ Nanostructures. *Applied Physics Letters*, **97**, 052902. http://dx.doi.org/10.1063/1.3475420

[12] Wang, Y., Hu, J., Lin, Y. and Nan, C.W. (2010) Multiferroic Magnetoelectric Composite Nanostructures. *NPG Asia Materials*, **2**, 61-68. http://dx.doi.org/10.1038/asiamat.2010.32

[13] Verma, V.K., Singh, V.R., Ishigami, K., Shibata, G., Harano, T., Kadono, T., Fujimori, A., Chang, F.-H., Lin, H.-J., Huang, D.J., Chen, C.T., Zhang, Y., Liu, J., Lin, Y., Nan, C.W. and Tanaka, A. (2014) Origin of Enhanced Magnetoelectric Coupling in NiFe$_2$O$_4$/BaTiO$_3$ Multilayers Studied by X-Ray Magnetic Circular Dichroism. *Physical Review B*, **89**, 115128. http://dx.doi.org/10.1103/PhysRevB.89.115128

[14] Zhang, Y., Deng, C.Y., Ma, J., Lin, Y.H. and Nan, C.W. (2008) Multiferroic Behaviour of Epitaxial NiFe$_2$O$_4$-BaTiO$_3$ Heterostructures. *Chinese Physics B*, **17**, 3910. http://dx.doi.org/10.1088/1674-1056/17/10/059

[15] Deng, C., Zhang, Y., Ma, J., Lin, Y. and Nan, C.W. (2008) Magnetoelectric Effect in Multiferroic Heteroepitaxial BaTiO$_3$-NiFe$_2$O$_4$ Composite Thin Films. *Acta Materialia*, **56**, 405-412. http://dx.doi.org/10.1016/j.actamat.2007.10.004

[16] Zhai, J., Dong, S., Xing, Z., Li, J. and Viehland, D. (2006) Giant Magnetoelectric Effect in Metglas/Polyvinylidene-Fluoride Laminates. *Applied Physics Letters*, **89**, 083507-1-3. http://dx.doi.org/10.1063/1.2337996

[17] Eiras, J.A., Gerbasi, R.B., Rosso, J.M., Silva, D.M., Cótica, L.F., Santos, I.A., Souza, C.A. and Lente, M.H. (2016) Compositional Design of Dielectric, Ferroelectric and Piezoelectric Properties of (K, Na)NbO$_3$ and (Ba, Na)(Ti, Nb)O$_3$ Based Ceramics Prepared by Different Sintering Routes. *Materials*, **9**, 179. http://dx.doi.org/10.3390/ma9030179

[18] Chaisan, W. (2007) Effect of Sintering Temperature on the Hysteresis Properties of Barium Titanate Ceramic. *NU Science Journal*, **4**, 132-139.

[19] Patil, D.R., Zhou, Y., Kang, J.E., Sharpes, N., Jeong, D.Y., Kim, Y.D., Kim, K.H., Priya, S. and Ryu, J. (2014) Anisotropic Self-Biased Dual-Phase Low Frequency Magneto-Mechano-Electric Energy Harvesters with Giant Power Densities. *APL Materials*, **2**, 046102-1-8. http://dx.doi.org/10.1063/1.4870116

[20] Mandal, S.K., Sreenivasulu, G., Petrov, V.M. and Srinivasan, G. (2010) Flexural Deformation in a Compositionally Stepped Ferrite and Magnetoelectric Effects in a Composite with Piezoelectrics. *Applied Physics Letters*, **96**, 192502-1-3. http://dx.doi.org/10.1063/1.3428774

[21] Fei, F., Peng, Z.C. and Wei, Y. (2011) Thickness Effects on Magnetoelectric Coupling Formetglas/PZT/Metglas Laminates. *Science China Physics*, *Mechanics & Astronomy*, **54**, 581-585. http://dx.doi.org/10.1007/s11433-011-4268-2